2021 10th International IEEE/EMBS Conference on Neural Engineering (NER)
Virtual Conference, May 4-6, 2021

# Real-Time Optimization of the Current Steering for Visual Prosthesis*

Zhijie Charles Chen[1], Bing-Yi Wang[2], and Daniel Palanker[3]

***Abstract*— Current steering on a multi-electrode array is commonly used to shape the electric field in the neural tissue in order to improve selectivity and efficacy of stimulation. Previously, simulations of the electric field in tissue required separate computation for each set of the stimulation parameters. Not only is this approach to modeling time-consuming and very difficult with a large number of electrodes, it is incompatible with real-time optimization of the current steering for practical applications. We present a framework for efficient computation of the electric field in the neural tissue based on superposition of the fields from a pre-calculated basis. Such linear algebraic framework enables optimization of the current steering for any targeted electric field in real time. For applications to retinal prosthetics, we demonstrate how the stimulation depth can be optimized for each patient based on the retinal thickness and separation from the array, while maximizing the lateral confinement of the electric field essential for high spatial resolution.**

## I. Introduction

For restoration of vision to the blind, an array of electrodes is placed in either the epiretinal or subretinal location, or on the visual cortex of the patient. Prosthetic vision of high fidelity requires selective neural stimulation, which is limited by the density of the electrode array and the crosstalk between neighboring electrodes. Crosstalk can be minimized by placement of the local return electrodes in each pixel, but this reduces the penetration depth of electric field into tissue. As a result, retinal stimulation with pixels smaller than about $50\,\mu\mathrm{m}$ becomes nearly impossible [1]. Crosstalk can also be reduced by time multiplexing – separating a video frame into multiple sparser sub-frames applied sequentially. However, the number of sub-frames is limited by the frame rate and by the pulse width required for neural stimulation. Another challenge is that neurons in the retina vastly outnumber the electrodes in the array, which limits the number of selective targets for stimulation. For example, the state-of-the-art photovoltaic retinal prosthesis (PRIMA, Pixium Vision) with $378$ pixels targets an area of $2\,\mathrm{mm}\times 2\,\mathrm{mm}$ in the macula [2], populated by at least $40\,000$ bipolar cells. Such discrepancy is even more significant for cortical implants, where the interface is 3-dimensional.

Current steering, a technique that utilizes simultaneous injection of current through multiple electrodes to shape the electric field in tissue, has been introduced to improve either the selectivity or efficacy of stimulation. It is used in cochlear implants [3][4][5], in deep-brain stimulation (DBS) [6][7][8][9] and in suprachoroidal implants [10][11][12] to enhance the stimulation capabilities with very limited number of electrodes, including creation of the "virtual electrodes" - centers of stimulation between the physical electrodes [4][10][11]. It was also used to direct current across the highly resistive retinal pigmented epithelium (RPE) layer [12]. In cortical visual prosthesis, current steering was implemented to provide smooth transition between the sequentially activated electrodes [13].

Computation of the electric field emanating from multiple electrodes involves Poisson's equation of volume conduction, which can be solved with the finite element method (FEM) [3][6][7][10][11][12]. In principle, for a certain optimization of the field confinement, the FEM, which takes at least several seconds to run on a typical computer, needs to be repeated for a very large number of the current settings on multiple electrodes. The computational cost increases with the total number of possible configurations, and would be intractable with even a few electrodes, each having tens of possible levels of current injection. Although iterative algorithms, such as gradient descent, may accelerate the convergence to the optimum, the FEM still needs to run for a number of times, thus precluding the FEM-based optimization for a video stream in real time, where the frame rate is typically in tens of $\mathrm{Hz}$ and the computation must be completed within tens of milliseconds. For application in visual prosthesis, predetermination of all possible stimulation schemes is impossible due to the large variety of visual scenes. Therefore, an efficient approach to real-time optimization of the current steering for visual prosthesis is required.

Since electric conduction in the tissue is typically linear (conductivity does not change with electric field) [14], and by the principle of superposition, the electric field is a weighted sum of the electric fields generated by each electrode individually, we may construct a dictionary comprising the elementary electric fields produced by each electrode with a unitary current, and calculate the actual electric field by linear combination of all dictionary entries, with coefficients equal to the respective currents. Similar approach was taken by [15] in modeling transcranial direct current stimulation. Although initial computation is required to generate the dictionary, all

*Research supported by the National Institutes of Health (Grants R01-EY-027786, P30-EY-026877), the Department of Defense (Grant W81XWH-19-1-0738), AFOSR (Grant FA9550-19-1-0402), Wu Tsai Institute of Neurosciences at Stanford.

[1]Z. C. Chen is with the Department of Electrical Engineering and Hansen Experimental Physics Laboratory at Stanford University, Stanford, CA 94305 USA zcchen@stanford.edu

[2]B.-Y. Wang is with the Department of Physics and Hansen Experimental Physics Laboratory at Stanford University, Stanford, CA 94305 USA bingyiw@stanford.edu

[3]D. Palanker is with the Department of Ophthalmology and Hansen Experimental Physics Laboratory at Stanford University, Stanford, CA 94305 USA palanker@stanford.edu

2021 10th International IEEE/EMBS Conference on Neural Engineering (NER) | 978-1-7281-4337-8/21/$31.00 ©2021 IEEE | DOI: 10.1109/NER49283.2021.9441400

possible electric fields could be rapidly synthesized without further running the FEM. Given the specifications of a targeted electric field, we can then find the best approximation of the current steering scheme under the minimum-mean-square-error (MMSE) criterion. We demonstrate a method for real-time optimization of current steering, and its utility for subretinal implants to find the optimal activation schemes that extend the stimulation into different depths of the inner nuclear layer (INL), while maintaining lateral confinement of electric field for high spatial resolution.

## II. The System Model

### A. A Basis for the Electric Field Computations

Let us consider an array of $M$ active electrodes interfacing with a volume of neural tissue $T$, which is the retina or the visual cortex, depending on the application. The surfaces with the electrodes in $T$ are denoted by $S_1, S_2, \cdots, S_M$ with surface areas of $s_1, s_2, \cdots, s_M$, respectively. $\varphi(\boldsymbol{r})$ denotes the potential distribution in the tissue as a function of the spatial variable $\boldsymbol{r}$. We choose $\varphi(\|\boldsymbol{r}\| \to +\infty) = 0$ and define $\hat{\boldsymbol{n}}_m$ as the normal to $S_m$, where $m \in \{1, 2, \cdots, M\}$.

The current injection of the $m^{\text{th}}$ electrode $I_m$ sinks to the return electrode $S'_m$, with area $s'_m$ and normal $\hat{\boldsymbol{n}}'_m$. $I_m$ can be either positive or negative, so the polarities of the electrodes are not predefined, and we adopt the convention of $I_m > 0$ for anodal stimulation. All the return electrodes may be connected as a common ground, so the notation does not imply that pixels are organized into bipolar pairs of the active and return electrodes. We assume a uniform current density (secondary current distribution) at the electrode-electrolyte interfaces, which is common in neural stimulation [16]. The framework can be easily adapted for other boundary conditions at the electrode surface, such as the primary or tertiary current distribution [17].

Let $\boldsymbol{\sigma}$ be the conductivity of the neural tissue, which may vary spatially in a non-uniform tissue, or be a tensor in anisotropic medium [9]. By the Poisson's equation for volume conduction, we have

$$\nabla(\boldsymbol{\sigma}\nabla\varphi) = 0. \tag{1}$$

The boundary conditions are

$$\lim_{\|\boldsymbol{r}\|\to+\infty} \varphi(\boldsymbol{r}) = 0, \tag{2a}$$

$$-(\boldsymbol{\sigma}\nabla\varphi)\cdot\hat{\boldsymbol{n}}_m = \frac{I_m}{s_m} \quad \text{at } S_m, \tag{2b}$$

and

$$-(\boldsymbol{\sigma}\nabla\varphi)\cdot\hat{\boldsymbol{n}}'_m = -\frac{I_m}{s'_m} \quad \text{at } S'_m \tag{2c}$$

for all $m$, and

$$(\boldsymbol{\sigma}\nabla\varphi)\cdot\hat{\boldsymbol{n}} = 0 \tag{2d}$$

at all inactive surfaces. In practice, (2a) can be imposed by a grounded bounding box that is much larger than the region of interest (ROI).

The equation system defined by (1) and (2) is linear with respect to $I_m$. Therefore, all possible electric fields in the neural tissue constitute an $M$-dimensional vector space. Let $I_0$ be the unitary current, and $\varphi_k$ be the potential distribution defined by (1) and (2) when

$$I_m = \begin{cases} I_0, & \text{if } m = k; \\ 0, & \text{if } m \neq k, \end{cases} \tag{3}$$

which is the potential distribution generated by the $k^{\text{th}}$ electrode injecting $I_0$ of current individually. $\{\varphi_1, \varphi_2, \cdots, \varphi_M\}$ forms a basis of the vector space. By the principle of superposition, we have

$$\varphi = \frac{1}{I_0}\sum_m \varphi_m I_m. \tag{4}$$

Thereby, we construct a dictionary of the elementary electric fields $\{\varphi_m\}$, from which all possible electric fields can be synthesized by linear combination with the currents at the electrodes as the coefficients. Note that the elementary electric fields are specific to the application, which may not require the granularity of a single electrode. For example, when the $40\,\mu\text{m}$-pixel photovoltaic subretinal implant described by [18] is used to determine grating acuity, it involves line-by-line activation of pixels. In this case, the dictionary consists of the electric fields generated by all the pixels uniformly activated in each line. This reduces the number of entries in such a dictionary from $425$ (the number of pixels) to only $35$ (the number of lines).

Storage of the dictionary can be resource-demanding, especially with a large number of electrodes. However, rarely is the case that potential distribution in the entire space is of interest. Usually only a subset of metrics is relevant for the application, such as the potential drop across a certain region. As long as the metrics are linearly derived from the electric field, storage of the entire electric field is unnecessary. We can first derive the metrics from the elementary electric fields, and then construct the dictionary with only the metrics of interest. For example, if we are interested in the potential difference $\Delta V$ between the dendritic and the axonal ends of a bipolar cell, the dictionary only needs to store the potential difference $\Delta V_m$ derived from each elementary electric field $\varphi_m$, and $\Delta V$ is given by

$$\Delta V = \frac{1}{I_0}\sum_m \Delta V_m I_m. \tag{5}$$

### B. Model of a Subretinal Implant

Fig. 1a illustrates a subretinal implant with active electrodes arranged in a 2-dimensional grid of $20\,\mu\text{m}$ in pitch, with a common distal ground electrode. Each active electrode is a disk of $8\,\mu\text{m}$ in diameter, and the electrode array is $1.5\,\text{mm}\times1.5\,\text{mm}$ in size, resembling the $20\,\mu$m-pixel device described in [18]. The retina has a thickness of $100\,\mu\text{m}$, a conductivity of $1\,\text{mS}\,\text{cm}^{-1}$ [19] and conductivity of the vitreous body above the retina is $11.3\,\text{mS}\,\text{cm}^{-1}$ [20].

The stimulation paradigm is configured by the currents at several neighboring electrodes. For example, let us consider a central electrode and the two neighboring electrodes on both sides. The dictionary will contain three elementary fields,

from which we can synthesize various linear combinations for different stimulation paradigms. When current of the same polarity is passed through each electrode, the stimulation is monopolar, with deep penetration and minimal lateral confinement of the electric field (Fig. 1b); when currents at the side electrodes have half of the amplitude and opposite polarity of the central electrode, the stimulation is bipolar (Fig. 1c), with the electric field penetrating shallower into the retina but more confined laterally; changing the ratio of currents between the side electrodes shifts the center of stimulation away from the central electrode, and hence creating the putative virtual electrode (Fig. 1d). Optimization of the currents at the electrodes for a targeted pattern yields stimulation beyond the simple monopolar and bipolar paradigms, and thus enables laterally confined electric fields at various penetration depths, which we will demonstrate in Section III-C.

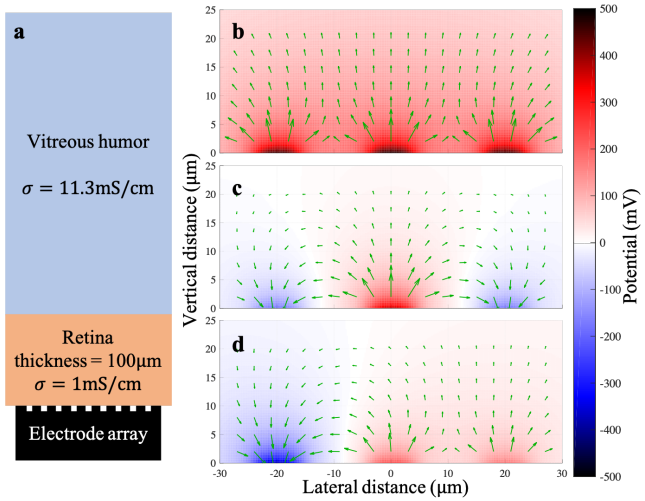


Fig. 1. (a) Schematic diagram of an implant under the degenerate retina in the eye. (b) Monopolar stimulation with $0.5\,\mu$A of current at each electrode. (c) Bipolar stimulation with $0.5\,\mu$A at the center electrode, and $-0.25\,\mu$A at each of the side electrodes. (d) Virtual electrode created at the center-right by $-0.5$, $0.3$ and $0.2\,\mu$A at the left, center and right electrode, respectively. (b)-(d) are synthesized by linear combination of the three elementary electric fields.

## III. Real-Time Optimization

To optimize the current steering scheme for each frame of the video stream, we need to specify the desired electric field. For example, a subretinal implant should depolarize the bipolar cells in the target region by creating a potential difference between the dendritic and the axon-terminal ends of the cells [19], while keeping the depolarization outside the target region as low as possible. Each scalar metric of the electric field is one specification (e.g. the potential at a certain point or the potential difference between two points), but a 3-dimensional variable (e.g. the current density at a point) should be considered three specifications.

### A. The Optimal Current Steering without Regularization

For illustration, let us consider the problem of defining the potential differences between the dendritic and the axon-terminal ends of bipolar cells at $L$ different locations, with $M$ subretinal electrodes. Let $V_l$ be the specification for the potential difference at the $l^{\text{th}}$ location, and $u_{l,m}$ be the potential difference at the $l^{\text{th}}$ location in the elementary electric field $\varphi_m$. Define $\boldsymbol{U}$ as the matrix with entry $u_{l,m}$ at row $l$ and column $m$, and $\boldsymbol{v}$ as the column vector whose $l^{\text{th}}$ component is $V_l$. We aim to find the currents at the electrodes $\boldsymbol{x} = [I_1, I_2, \cdots, I_M]^\intercal$ that generate an electric field closest to the specifications under the MMSE criterion, such that

$$\min_{\boldsymbol{x}} \|\boldsymbol{U}\boldsymbol{x} - \boldsymbol{v}\|^2. \tag{6}$$

When the number of specifications is smaller than the number of independent electrodes ($L < M$), the problem is underdetermined. Since we have more "tuning knobs" than specifications, all specifications can be satisfied and the minimum of (6) is 0. The solution to (6) is given by

$$\boldsymbol{x}^* = \boldsymbol{U}^\intercal(\boldsymbol{U}\boldsymbol{U}^\intercal)^{-1}\boldsymbol{v} + \boldsymbol{w}, \tag{7}$$

where $\boldsymbol{w}$ is any vector in the nullspace of $\boldsymbol{U}$. Because the solution is not unique, we may optimize for other criteria. For example, the sum of squares of all currents reflects the total power consumption. Therefore, minimal power consumption is achieved if and only if $\boldsymbol{w} = \boldsymbol{0}$.

When there are more specifications than electrodes, the problem is overdetermined. Generally, all specifications cannot be met simultaneously, and the optimal current steering scheme under the MMSE criterion, $\boldsymbol{x}^*$, is given by

$$\boldsymbol{x}^* = (\boldsymbol{U}^\intercal\boldsymbol{U})^{-1}\boldsymbol{U}^\intercal\boldsymbol{v}. \tag{8}$$

### B. Regularized Optimal Current Steering

A common problem of optimization is over-fitting, which typically results in coefficients with unreasonably large amplitudes. Because the current injection capacity of each electrode is limited, over-fitting in the optimization of current steering should be avoided, and we propose adding the Tikhonov regularization term in (6) to limit the amplitudes of the coefficients in $\boldsymbol{x}$:

$$\min_{\boldsymbol{x}}\{\|\boldsymbol{U}\boldsymbol{x} - \boldsymbol{v}\|^2 + \lambda^2\|\boldsymbol{x}\|^2\}, \tag{9}$$

where $\lambda^2$ is the ridge parameter we can control to penalize large coefficients. The regularized optimal solution $\boldsymbol{x}^*$ to (9) is given by

$$\boldsymbol{x}^* = \left(\boldsymbol{U}^\intercal\boldsymbol{U} + \lambda^2\boldsymbol{I}\right)^{-1}\boldsymbol{U}^\intercal\boldsymbol{v}, \tag{10}$$

where $\boldsymbol{I}$ is the identity matrix.

The multipliers on the left of $\boldsymbol{v}$ in (7), (8) and (10) are pre-calculated matrices and do not change with the image frame. The real-time computation for the optimal current steering scheme involves only one matrix-vector multiplication, which makes the computation highly efficient.

### C. Stimulation Depth and Lateral Field Confinement

To achieve prosthetic visual acuity matching the sampling limit of the electrode array, lateral confinement of the electric field is required to suppress crosstalk between the electrodes. However, lateral confinement with local returns also limits the penetration of electric field into the retina. Small bipolar pixels over-constrain the field penetration to less than a pixel radius and thus strongly diminish the stimulation efficacy [21]. We may laterally confine the electric field more efficiently with current steering. Using the theory developed in Section III-A and III-B, we now optimize for the current steering schemes for selective stimulation of the INL at various depths with the subretinal implant described in Section II-B.

Let us assume that activation of a bipolar cell is determined by the potential difference between its two ends [19], and that its length is $35\,\mu\mathrm{m}$. Let us also assume that proximity between the implant and the dendritic ends of the bipolar cells, denoted by $z_0$, varies between patients, and we will model three scenarios where $z_0$ equals 5, 25 and $45\,\mu\mathrm{m}$, respectively. The ROI is a $100\,\mu\mathrm{m}$-wide square concentric to the implant, in which we configure the potential difference between $z_0$ and $z_0{+}35\,\mu\mathrm{m}$ with 141 electrodes near the center of the implant. The targeted potential difference is a 2-dimensional boxcar function, where the value is $50\,\mathrm{mV}$ in the central square of $40\,\mu\mathrm{m}$ in width and $0\,\mathrm{mV}$ elsewhere. The ROI is discretized in steps of $0.5\,\mu\mathrm{m}$, yielding $201{\times}201$ sampling points and thus $40\,401$ specifications. The problem is overdetermined, and we aim to find the optimal current steering schemes that selectively activate the central square at different depths, with and without the regularization. We empirically choose $\lambda = 50\,\mathrm{k}\Omega$ for the ridge parameter.

Fig. 2 compares the lateral confinement of the electric field by the optimal current steering with and without the regularization at three stimulation depths, with that by direct spatial modulation, where only the electrodes in the central square are activated. Optimal current steering confines the electric field much better at all stimulation depths, especially at deeper target layers. However, the current amplitude of optimal current steering without regularization is much higher than that of direct spatial modulation, as shown in Table III-C. With regularization, the current amplitude is significantly reduced at the price of minor compromise of the field confinement. The ridge parameter $\lambda^2$ determines the trade-off between meeting the specifications and limiting the current amplitudes.

TABLE I

AVERAGE CURRENT AMPLITUDE OF THE ELECTRODES

| $z_0$ (μm) | 5 | 25 | 45 |
|---|---|---|---|
| Opt. w/o regularization | 5.10 μA | 5.10 μA | 6.35 μA |
| Opt. w/ regularization | 0.11 μA | 0.12 μA | 0.28 μA |
| Direct spatial modulation | 0.02 μA | 0.07 μA | 0.12 μA |

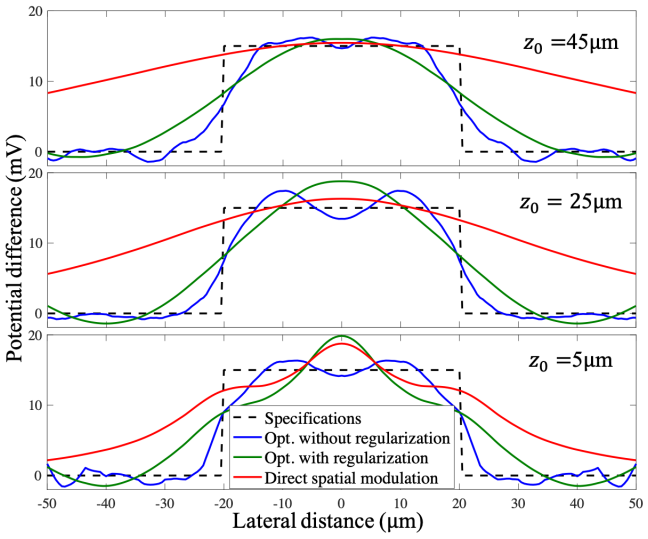


Fig. 2. Lateral confinement of the electric field at three stimulation depths. Top: potential difference between 45 and 80 μm from the implant; Middle: 25 to 60 μm; Bottom: 5 to 40 μm.

## IV. Discussion

Equations (7), (8) and (10) show that the real-time optimization for each frame requires only one matrix-vector multiplication, which is a basic operation that has been extensively optimized in many software packages. The optimization in Section III-C involves 141 electrodes and 40 401 specifications of the targeted electric field, yet takes only 2 ms to run on a laptop computer (3.1 GHz dual-core CPU, 8 GB memory) with MATLAB (64-bit R2017a, Mathworks Inc.), meeting the requirement for real-time implementation. The matrix-vector multiplication can further benefit from hardware acceleration using field-programmable gate array (FPGA) or application-specific integrated circuit (ASIC).

Although optimization of the current steering we propose is highly efficient, construction of the dictionary could be time consuming with a large number of electrodes, since each elementary electric field still requires one FEM simulation. However, we may exploit the symmetry and invariance in the geometry of the electrode array to simplify the process. For example, for the optimization in Section III-C, since all the engaged electrodes are near the center of an implant which is much larger than the ROI, the edge effects are negligible, and thus the elementary fields are space-shifted versions of each other. Thereby, the FEM simulation only needs to run once.

In patients with subretinal implants, the critical trade-off between the stimulation depth and lateral confinement of the electric field depends on the proximity between the INL and the implant, which varies between patients and is affected by multiple factors, such as post-surgical retinal reattachment, potential retinal edema, state of degeneration, and others. With local returns around each active electrode to confine the field, different patients would require implants with different pixel sizes that may not even be known before

the implantation. The optimal current steering provides an approach to adjustment of the stimulation depth by software, thus accommodating all patients with a single design of the implant.

With the optimal current steering, deep penetration of the electric field does not necessarily compromise the lateral selectivity. Section III-C demonstrates a boxcar function of the same width at different depths of the INL. A sharp boxcar function is an important building block for representing a complex image as multiple sparse sub-frames, which are sequentially activated within a frame duration. The maximum number of sub-frames is determined by the ratio of the frame duration ($1/$frame rate) to pulse duration required for neural stimulation. The optimization we propose enables sufficiently fast computation to fit the requirement not only for a video rate, but also for the time multiplexing with the sub-frame duration in the range of a few milliseconds.

This framework and the optimization may also be used in other areas of neural stimulation, such as cochlear implants and DBS, for example.

## V. Conclusions

A framework was proposed to efficiently model and optimize for the current steering in neural tissues by linear combination of a set of pre-calculated elementary electric fields. Such approach to finding the optimal current steering scheme for any targeted electric field can be implemented in real time. We demonstrated a utility of such optimization for subretinal implants to stimulate the INL at different depths while maintaining a constant lateral confinement, thereby overcoming the limitation on penetration depth of the electric field imposed by the fixed local return electrodes.

## References


[1] E. Ho, X. Lei, T. Flores, H. Lorach, T. Huang, L. Galambos, T. Kamins, J. Harris, K. Mathieson, and D. Palanker, "Characteristics of prosthetic vision in rats with subretinal flat and pillar electrode arrays," *Journal of neural engineering*, vol. 16, no. 6, p. 066027, 2019.

[2] D. Palanker, Y. Le Mer, S. Mohand-Said, M. Muqit, and J. A. Sahel, "Photovoltaic restoration of central vision in atrophic age-related macular degeneration," *Ophthalmology*, 2020.

[3] B. H. Bonham and L. M. Litvak, "Current focusing and steering: modeling, physiology, and psychophysics," *Hearing research*, vol. 242, no. 1-2, pp. 141–153, 2008.

[4] J. B. Firszt, D. B. Koch, M. Downing, and L. Litvak, "Current steering creates additional pitch percepts in adult cochlear implant recipients," *Otology & Neurotology*, vol. 28, no. 5, pp. 629–636, 2007.

[5] C.-C. Wu and X. Luo, "Current steering with partial tripolar stimulation mode in cochlear implants," *Journal of the Association for Research in Otolaryngology*, vol. 14, no. 2, pp. 213–231, 2013.

[6] C. T. Choi, Y.-T. Lee, and Y.-L. Tsou, "Modeling deep brain stimulation based on current steering scheme," *IEEE transactions on magnetics*, vol. 47, no. 5, pp. 890–893, 2011.

[7] A. Chaturvedi, T. J. Foutz, and C. C. McIntyre, "Current steering to activate targeted neural pathways during deep brain stimulation of the subthalamic region," *Brain stimulation*, vol. 5, no. 3, pp. 369–377, 2012.

[8] M. T. Barbe, M. Maarouf, F. Alesch, and L. Timmermann, "Multiple source current steering–a novel deep brain stimulation concept for customized programming in a parkinson's disease patient," *Parkinsonism & Related Disorders*, vol. 20, no. 4, pp. 471–473, 2014.

[9] S. Zhang, P. Silburn, N. Pouratian, B. Cheeran, L. Venkatesan, A. Kent, and A. Schnitzler, "Comparing current steering technologies for directional deep brain stimulation using a computational model that incorporates heterogeneous tissue properties," *Neuromodulation: Technology at the Neural Interface*, vol. 23, no. 4, pp. 469–477, 2020.

[10] G. Dumm, J. B. Fallon, C. E. Williams, and M. N. Shivdasani, "Virtual electrodes by current steering in retinal prostheses," *Investigative ophthalmology & visual science*, vol. 55, no. 12, pp. 8077–8085, 2014.

[11] T. C. Spencer, J. B. Fallon, and M. N. Shivdasani, "Creating virtual electrodes with 2d current steering," *Journal of neural engineering*, vol. 15, no. 3, p. 035002, 2018.

[12] P. B. Matteucci, S. C. Chen, D. Tsai, C. W. Dodds, S. Dokos, J. W. Morley, N. H. Lovell, and G. J. Suaning, "Current steering in retinal stimulation via a quasimonopolar stimulation paradigm," *Investigative ophthalmology & visual science*, vol. 54, no. 6, pp. 4307–4320, 2013.

[13] M. S. Beauchamp, D. Oswalt, P. Sun, B. L. Foster, J. F. Magnotti, S. Niketeghad, N. Pouratian, W. H. Bosking, and D. Yoshor, "Dynamic stimulation of visual cortex produces form vision in sighted and blind humans," *Cell*, vol. 181, no. 4, pp. 774–783, 2020.

[14] Z. C. Chen, B.-Y. Wang, and D. Palanker, "Harmonic-balance circuit analysis for electro-neural interfaces," *Journal of Neural Engineering*, 2020.

[15] J. P. Dmochowski, A. Datta, M. Bikson, Y. Su, and L. C. Parra, "Optimized multi-electrode stimulation increases focality and intensity at target," *Journal of neural engineering*, vol. 8, no. 4, p. 046011, 2011.

[16] Z. Chen, L. Ryzhik, and D. Palanker, "Current distribution on capacitive electrode-electrolyte interfaces," *Physical Review Applied*, vol. 13, no. 1, p. 014004, 2020.

[17] B. Wang and J. D. Weiland, "Review of newman's analytical series on disk electrodes," *arXiv preprint arXiv:1908.00051*, 2019.

[18] T. W. Huang, T. I. Kamins, Z. C. Chen, B.-Y. Wang, M. B. Bhuckory, L. Galambos, E. Ho, T. Ling, S. Afshar, A. Shin, *et al.*, "Vertical-junction photodiodes for high-resolution retinal prostheses," *Journal of neural engineering*, 2021, in press https://doi.org/10.1088/1741-2552/abe6b8.

[19] P. Werginz, B.-Y. Wang, Z. C. Chen, and D. Palanker, "On optimal coupling of the 'electronic photoreceptors' into the degenerate retina," *Journal of Neural Engineering*, vol. 17, no. 4, p. 045008, 2020.

[20] A. Oksala and A. Lehtinen, "Comparative studies on the electrical conductivity of aqueous humour, vitreous body, cornea and sclera," *Acta ophthalmologica*, vol. 37, no. 4, pp. 388–394, 1959.

[21] T. Flores, T. Huang, M. Bhuckory, E. Ho, Z. Chen, R. Dalal, L. Galambos, T. Kamins, K. Mathieson, and D. Palanker, "Honeycomb-shaped electro-neural interface enables cellular-scale pixels in subretinal prosthesis," *Scientific reports*, vol. 9, no. 1, pp. 1–12, 2019.